

1 **Global Nitrogen and Sulfur Deposition Mapping Using a**  
2 **Measurement-Model Fusion Approach**

Deleted: Budgets

3 **Hannah J. Rubin<sup>1</sup>, Joshua S. Fu<sup>1,2</sup>, Frank Dentener<sup>3</sup>, Rui Li<sup>4</sup>, Kan Huang<sup>5</sup>, Hongbo Fu<sup>5</sup>**

4 <sup>1</sup>Department of Civil and Environmental Engineering, University of Tennessee, Knoxville, TN, 37996, USA

5 <sup>2</sup>Computational Earth Science Group, Oak Ridge National Laboratory, Oak Ridge, TN 37831, USA

6 <sup>3</sup>European Commission, Joint Research Centre, [Sipra](#), Italy

Deleted: Ispra

7 <sup>4</sup>Ministry of Education Key Laboratory for Earth System Modeling, Department of Earth System Science, Tsinghua  
8 University, Beijing, 100084, China

9 <sup>5</sup>Shanghai Key Laboratory of Atmospheric Particle Pollution and Prevention (LAP3), Department of Environmental  
10 Science and Engineering, Fudan University, Shanghai, 200433, China

11 E-mail: [jifu@utk.edu](mailto:jifu@utk.edu)

12  
13  
14 **Keywords:** Measurement-model fusion, nitrogen deposition, [sulphur](#) deposition, HTAP II,  
15 ammonia, multiple-model mean

Deleted: sulfur

16

20 **Abstract**

21 Global reactive nitrogen (N) deposition has more than tripled since 1860 and is expected to  
22 remain high due to [food production](#) and fossil fuel consumption. We update the 2010 global  
23 deposition budget for [reactive](#) nitrogen and sulfur [components](#) with new regional wet deposition  
24 measurements from Asia, improving the ensemble results of eleven global chemistry transport  
25 models from the second phase of the United Nation’s Task Force on Hemispheric Transport of  
26 Air Pollution (HTAP-II). [The observationally adjusted global N deposition budget is 114.5 Tg-](#)  
27 [N, representing a minor increase of 1 % from the model-only derived values, and the adjusted](#)  
28 [global sulfur deposition budget is 88.9 Tg-S, representing a 6.5% increase from the modelled](#)  
29 [values, using an interpolation distance of 2.5 degrees. Regionally, deposition adjustments can be](#)  
30 [up to ~73% for nitrogen, and 112% for sulfur. Our study demonstrates that a global](#)  
31 [measurement-model fusion approach can improve N and S deposition model estimates at a](#)  
32 [regional scale, with sufficient availability of observations, but in large parts of the world,](#)  
33 [alternative approaches need to be explored. The analysis presented here represents a step forward](#)  
34 [toward the World Meteorological Organization’s goal of global fusion products for accurately](#)  
35 [mapping harmful air pollution deposition.](#)

Deleted: land use changes

Deleted: 0

Deleted: no change

Deleted: led

Deleted: 1

Deleted: adjustments

Deleted: xx

Deleted:

Deleted: yy

Deleted: and

37 **1. Introduction**

38 Atmospheric nitrogen and sulfur deposition from human activities related to the use of fossils  
39 and land use have significant implications for ecosystem and human health.  
40 . Elevated levels of nitrogen and sulfur can lead to eutrophication (Anderson et al., 2008; Heisler  
41 et al., 2008), changes in carbon sequestration (Kicklighter et al., 2019; de Vries et al., 2009; Zhu  
42 et al., 2020), loss of biodiversity (Clark et al., 2013; Dise and Stevens, 2005), and acidification  
43 (Bowman et al., 2008). While sulfur deposition is expected to decrease over the next 80 years  
44 (Lamarque et al., 2013), it will remain a serious hazard in many emerging economies. For  
45 instance, sulfur deposition in East Asia peaked in 2006 (Lu et al., 2010) but is still high enough  
46 to be concerning, especially in natural and semi-natural regions (Doney et al., 2007; Luo et al.,  
47 2014).

Deleted: The observationally adjusted global N deposition budget is 130 Tg-N, representing a 10% increase and the adjusted global sulfur deposition budget is 80 Tg-S, representing no change. Our study demonstrates that a global measurement-model fusion approach can substantially improve N and S deposition model estimates at a regional scale and represents a step forward toward the World Meteorological Organization’s goal of global fusion products for accurately mapping harmful air pollution deposition.

Deleted: (Bobbink et al., 2010)

48 Oxidized nitrogen ( $\text{NO}_{\text{SV}}$ ) and reduced nitrogen ( $\text{NH}_x$ ), together called reactive nitrogen (Nr), and  
49 oxidized sulfur ( $\text{SO}_x$ ) deposition occur as wet and dry processes (Dentener et al., 2006). Wet

Deleted:  $\text{NO}_y$

71 deposition is measured at hundreds of locations in Europe, North America, and Asia, but dry  
72 deposition is harder to measure and is often instead derived from ambient concentrations and  
73 modeled deposition velocities (Xu et al., 2015). For example, dry deposition is inferred from  
74 continuous concentration measurements combined with modeled dry deposition velocities at a  
75 few locations in North America (Clean Air Status and Trends Network (CASTNET), 2021) and  
76 Asia (Acid Deposition Monitoring Network in East Asia (EANET), 2021).

Deleted: D

Deleted: It

Deleted: estimated

77 The United Nations Economic Commission for Europe’s Task Force on Hemispheric Transport  
78 of Air Pollution (HTAP) is an international effort to improve the understanding of air pollution  
79 transport science with emissions models. The second phase of HTAP was launched in 2012. Tan  
80 et al. (2018) used the multi-model mean (MMM) of 11 HTAP II chemistry transport models to  
81 estimate the sulfur and nitrogen deposition budgets for 2010. Significant uncertainty remained  
82 due to a lack of station measurements, especially in East Asia, a large contributor to the overall  
83 budget. Tan et al. (2018) compared Acid Deposition Monitoring Network in East Asia (EANET  
84 (Acid Deposition Monitoring Network in East Asia, 2021)) measurements to the MMM output  
85 but there were very few measurements in East Asia and all were located along the southeastern  
86 coast. In contrast, the highest emissions and modeled deposition were inland and north, making it  
87 challenging to evaluate model performance.

Deleted: Tan et al.,

Deleted: Tan et al.,

88 Combining measurements and model estimates in a “measurement-model fusion” (MMF)  
89 approach has the advantage of retaining the broad spatial coverage of models while accurately  
90 matching observations. Generally speaking, MMF takes model estimates of concentrations or  
91 fluxes for a region and modifies them based on in-situ point measurements to force the model  
92 towards the observed values (Labrador et al., 2020). One global MMF approach for wet  
93 deposition combined measurements with HTAP I ensemble model values for 2000-2002 (Vet et  
94 al., 2014) where model estimates filled empty grid cells lacking a 3-year observed mean.  
95 Another MMF approach in North America (Atmospheric Deposition Analysis Generated from  
96 optimal Interpolation from Observations, “ADAGIO”) used observed concentrations to adjust  
97 predicted concentrations from the Global Environmental Multiscale-Modelling Air Quality and  
98 Chemistry (GEM-MACH) model (Schwede et al., 2019). Recent work in the US (Schwede and  
99 Lear, 2014; Zhang et al., 2019) incorporates Community Multiscale Air Quality (CMAQ) model  
100 output and precipitation data generated by the Parameter-elevation Regressions on Independent  
101 Slopes Model (PRISM, <https://prism.oregonstate.edu/>, Accessed: 10/01/22), as well as

Deleted: of the phenomenon

Deleted: “nudge”

109 observations using inverse distance weighting to create total deposition (“TDep”,  
 110 <https://nadp.slh.wisc.edu/committees/tdep/#tdep-maps>) maps that are publicly available.  
 111 More details of the MMF approach are described in Fu et al. (2022) as they lay out a roadmap  
 112 for future work, following the World Meteorological Organization’s Global Atmosphere Watch  
 113 Program (WMO GAW) and the intended role of the MMF Global Total Atmospheric Deposition  
 114 (MMF-GTAD) project. This study updates Tan et al.’s (2018) global S and N deposition  
 115 budgets using a variation of the TDep methodology (Schwede and Lear, 2014) to merge NH<sub>x</sub>,  
 116 NO<sub>y</sub>, and SO<sub>x</sub> modelled gridded deposition fluxes results with deposition fluxes derived from  
 117 observations of NO<sub>3</sub><sup>-</sup>, NH<sub>4</sub><sup>+</sup>, and SO<sub>4</sub><sup>2-</sup> in precipitation and precipitation amounts. The main  
 118 purpose of our study is to demonstrate the viability of a straightforward but globally applicable  
 119 MMF approach, while remaining consistent with previous work that provided datasets for impact  
 120 assessments for various communities. This approach is an important intermediate step towards  
 121 the WMO’s goal of reliable deposition products to aid decision-making. We update the 2010  
 122 deposition budgets using MMF to combine the broad spatial coverage of a model with accurate  
 123 in-situ measurements.

Deleted: Fu et al.,

Deleted: Tan et al.,

Deleted: surfaces from modeled

Deleted: .

Deleted: We

Deleted: s

Deleted: essential

## 124 2. Data Availability

125 **Table 1:** Sources of deposition observations.

Name	Source	Number of Observations	Region	Value
NTN, AIRMoN	NADP	247	USA	wet deposition
CASTNET	NADP	84	USA	dry deposition
CAPMoN	NAAtChem	27	Canada	wet and dry deposition
EMEP	EMEP	86	Europe	wet deposition
China Scientific Study	Li et al. 2019	407	China	wet deposition
EANET	EANET	47	East Asia	wet and dry deposition

IDAF	INDAAF	1	Niger	wet deposition
------	--------	---	-------	----------------

133

134 All data are from 2010, reported monthly with sources summarized in Table 1. Wet deposition  
135 measurements ( $\text{NO}_3^-$ ,  $\text{NH}_4^+$ , and  $\text{SO}_4^{2-}$ ) from the US's National Trends Network (NTN) and  
136 Atmospheric Integrated Research Monitoring Network (AIRMoN) are available through the  
137 National Atmospheric Deposition Program (NADP (National Atmospheric Deposition Program,  
138 2021), <http://nadp.slh.wisc.edu/NTN/>). Measurements were filtered for completeness and quality,  
139 following Schwede and Lear (2014). Sites without a full year of measurements or with quality  
140 tags indicating collection issues were not included, resulting in 247 observations in the US. Dry  
141 deposition generated values are available from the Clean Air Status and Trends Network  
142 (CASTNET, 2021) at 84 locations. CASTNET uses an inferential method to calculate dry  
143 deposition fluxes as a product of surface concentration and modeled dry deposition velocity.  
144 Nitrogen and sulfur wet deposition measurements and dry deposition estimates throughout  
145 Canada are recorded by the Canadian Air and Precipitation Monitoring Network (CAPMoN  
146 (2021), and are available through the National Atmospheric Chemistry (NAChem) database  
147 (<https://donnees.ec.gc.ca/data/air/monitor/>). Dry deposition estimates from CAPMoN are  
148 calculated by multiplying atmospheric concentration and deposition velocity. There were 27 sites  
149 with a full year of quality checked data for 2010.  
150 The European Monitoring and Evaluation Programme (EMEP (European Monitoring and  
151 Evaluation Programme (EMEP), 2021; Tørseth et al., 2012), <http://ebas-data.nilu.no/>) provides  
152 records of precipitation chemistry ( $\text{NO}_3^-$ ,  $\text{NH}_4^+$ , and  $\text{SO}_4^{2-}$ ) and precipitation depths for Europe.  
153 There were 86 sites with a full year of quality checked data in 2010.  
154 In China, a multi-year nationwide field study, including some of these NNDMN data, was  
155 compiled by Li et al. (2019). Daily  $\text{NO}_3^-$ ,  $\text{NH}_4^+$ , and  $\text{SO}_4^{2-}$  site measurements (in mg/L) were  
156 averaged for 2010 for each of the 407 site locations with complete records by multiplying the  
157 concentration by the precipitation recorded at that same site (in mm) and then aggregating to  
158 produce annual precipitation-weighted deposition (Sirois, 1990). For a wider Asian region,  
159 EANET (Asia Center for Air Pollution Research, 2021, <https://www.eanet.asia/>) wet and dry  
160 deposition and precipitation data are available at 47 sites.  
161 The International Global Atmospheric Chemistry (IGAC) Deposition of Biogeochemically  
162 Important Trace Species (DEBITS) Africa (IDAF) program (Adon et al., 2010; Galy-Lacaux et

**Deleted:** collected

**Deleted:** Schwede and Lear,

**Deleted:**

**Deleted:** (Clean Air Status and Trends Network

**Deleted:** (CASTNET),

**Deleted:** )

**Deleted:** (Canadian Air and Precipitation Monitoring Network, ...

**Deleted:** )

**Deleted:** has

**Moved down [1]:** A promising data set of wet deposition measurements ( $\text{NO}_3^-$ ,  $\text{NH}_4^+$ , and  $\text{SO}_4^{2-}$ ) in China is available through the National Nitrogen Deposition Monitoring Network (NNDMN (Xu et al., 2019)). It is comparable to other regional measurements (Wen et al., 2020). However, these data only exist for a fraction of 2010 (from September onwards) for a few sites; rather than use partial data to represent an entire year, these sites were not included.

**Deleted:** A

**Deleted:** prior

**Deleted:** Li et al.,

**Deleted:** , which was used in this work as a good proxy for use of NNDMN data in the future studies.

**Deleted:** over the year

**Moved (insertion) [1]**

**Deleted:** A promising data set of wet deposition measurements ( $\text{NO}_3^-$ ,  $\text{NH}_4^+$ , and  $\text{SO}_4^{2-}$ ) in China is available through the National Nitrogen Deposition Monitoring Network (NNDMN (Xu et al., 2019)). It is comparable to other regional measurements (Wen et al., 2020). However, these data only exist for a fraction of 2010 (from September onwards) for a few sites; rather than use partial data to represent an entire year, these sites were not included.¶

195 al., 2014) has  $\text{NH}_4^+$  and  $\text{NO}_3^-$  precipitation concentrations on the International Network to Study  
196 Deposition and Atmospheric Chemistry in Africa (INDAAF (INDAAF – International Network  
197 to study Deposition and Atmospheric chemistry in Africa, 2021)) website ([https://indaaf.obs-](https://indaaf.obs-<br/>198 mip.fr/)

199 All measurements were converted to  $\text{mg-N}$  (or  $\text{S}$ ) / $\text{m}^2/\text{yr}$ .

Deleted: .

### 200 3. Measurement Model Fusion Procedure

Deleted: Measurement

201 Global yearly wet and dry  $\text{NO}_3^-$ ,  $\text{NH}_4^+$ , and  $\text{SO}_4^{2-}$  deposition observations (for wet deposition) or  
202 estimates derived from near-surface concentrations and modelled deposition velocities for dry  
203 deposition) were combined with the respective HTAP II model average grid cell estimates, using  
204 model output interpolated to common 1 degree x 1 degree ( $1^\circ \times 1^\circ$ ) grid cells (Figure 1). For  
205 example, wet  $\text{NO}_3^-$  deposition observations are combined with the wet  $\text{NO}_3^-$  modeled deposition  
206 in the nearest HTAP II MMM grid cell to the observation, where observations exist. Dry  
207 deposition values ( $\text{NO}_3^-$ ,  $\text{NH}_4^+$ , and  $\text{SO}_4^{2-}$ ) from CASTNET and an inverse-distance weighted  $1^\circ$   
208  $\times 1^\circ$  gridded dataset was created based on the distance from each observation to the center of the  
209 nearest HTAP II model grid cell. Inverse-distance weighting (IDW) was selected as the most  
210 straight forward to implement method to introduce MMF on a global scale while remaining  
211 consistent with previous work (Schwede and Lear, 2014).

Deleted: (

212 The weighting function was calculated as

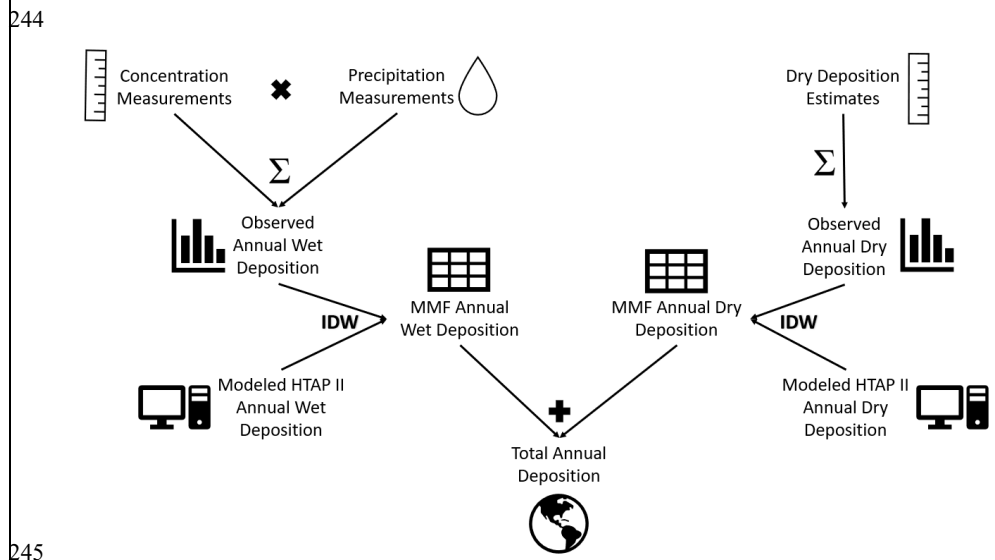
$$213 \left(1 - \frac{\text{distance}}{\text{max distance}}\right)^2 \quad (1)$$

214 following Schwede and Lear's (Schwede and Lear, 2014) approach for the TDep product, where  
215 "distance" is the distance between the site location and the center of the HTAP II model grid cell  
216 nearest to that sampling site location, within a maximum distance of  $2.5^\circ$  (approximately  $280 \text{ km}$   
217 at middle latitudes). The choice of the maximum distance is a crucial parameter for the inverse  
218 distance weighting method in MMF. Prior analysis (e.g. Tan et al. 2018b) has shown that  
219 gaseous and particulate sulfur and nitrogen emissions can travel several hundreds of kilometers,  
220 before being deposited, although there is likely to be a large variation of transport distances due  
221 to regional differences in chemistry, meteorological conditions, transport patterns and removal  
222 processes. These processes interact with spatially heterogeneous emissions. Since there will not  
223 be a single distance that captures the heterogeneity of all processes at play, we present here a

Deleted: 111

228 [base case using a 2.5° interpolation distance, and two sensitivity cases reducing the distance to 1°](#)  
 229 [and increasing it to 5°, respectively. The 5° distance can be seen as an upper limit for the distance](#)  
 230 [where deposition observations can constrain deposition.](#) The output values of the weighting  
 231 function at each observation location are then multiplied by the observed deposition. For the  
 232 center of every HTAP II model grid cell near that site, the modeled deposition is multiplied by 1  
 233 minus the value of the weighting function. [Consequently](#), if there are no observations near [the](#)  
 234 model grid cells, the cell value remains the same. The two grid [values](#) ([weighting function times  
 235 observed deposition] and [1-weighting function times modeled deposition]) are added together [to](#)  
 236 [give the value of the MMF estimate.](#) This has the effect of modifying the HTAP II grid [values](#)  
 237 only in locations where there are observations [within the maximum interpolation distance.](#)

238 The MMF gridded surfaces were then summed by species along with the remaining unchanged  
 239 HTAP II gridded surfaces that lacked in-situ measurements to create total N and S deposition  
 240 gridded surfaces (e.g., the MMF wet and dry SO<sub>4</sub><sup>-</sup> gridded surfaces were added to the HTAP II  
 241 wet and dry SO<sub>2</sub> gridded surfaces to get total S deposition). The MMF wet deposition surfaces  
 242 include measurements from Europe, Asia, and North America, [and](#) the dry deposition MMF  
 243 surfaces include [estimates](#) from the USA and Asia [\(see section 2\).](#)



Deleted: As a consequence

Deleted: a

Deleted: nearby

Deleted: but

Deleted: only

Deleted: measurements

Deleted: ,

Deleted: due to a lack of measurements elsewhere.

Figure 1. A flowchart describes the MMF methodology implemented in this paper.

#### 4. Results

The total global NH<sub>x</sub> deposition in 2010 increased from 54.0 Tg-N (from HTAP II models) to 54.9 Tg-N (Table 2). Combined with a NO<sub>y</sub> deposition of 59.6 Tg-N (from a modeled HTAP II 59.3 Tg-N), the total global deposition is adjusted to 114.5 Tg-N (from 113 Tg-N), an increase by 1%. While the IDW tends to decrease the depositions over the continents, an increase is calculated over coastal regions and open oceans using the 2.5x2.5 maximum distance. Total S deposition is adjusted to 88.91 Tg-S (Table 2), an increase by 6.5% from the HTAP II model prediction of 83.5 Tg-S (Figure 2B). Regional changes greater than or equal to 10% are bolded and italicized.

Table 2: 2010 adjusted global wet and dry deposition in Tg N or Tg S. MMM indicates Tan et al.'s 2018 multi-model mean and MMF is this measurement-model fusion work with a 2.5° interpolation distance. Coastal means deposition on sea within 1 degree of the coastline. RBU is an abbreviation for Russia, Belarus, and Ukraine. Open ocean does not include near-land "coastal" waters. The regions can be seen in the world map in Figure S1. Regional changes greater than or equal to 10% are bolded and italicized.

Region	Non-Coastal		Coastal		Non-Coastal		Coastal		Non-Coastal		Coastal	
	MMM	MMF	MMM	MMF	MMM	MMF	MMM	MMF	MMM	MMF	MMM	MMF
	<b>Total NH<sub>x</sub></b>				<b>Total NO<sub>y</sub></b>				<b>Total SO<sub>x</sub></b>			
North America	3.40	3.66	0.40	<b>0.31</b>	4.40	4.50	0.80	<b>0.94</b>	4.70	<b>5.67</b>	1.30	<b>1.69</b>
Europe	2.50	2.68	0.80	<b>1.14</b>	2.60	2.42	1.20	<b>1.75</b>	2.70	2.50	1.50	<b>3.18</b>
South Asia	8.60	8.60	1.00	1.00	3.60	3.60	0.70	0.70	3.70	3.70	1.00	1.00
East Asia	6.70	6.49	1.00	1.04	8.30	6.90	2.20	<b>2.45</b>	11.20	11.89	2.90	<b>4.10</b>
Southeast Asia	3.20	<b>2.22</b>	1.60	<b>2.12</b>	1.90	<b>1.60</b>	1.40	1.44	2.40	<b>0.81</b>	2.80	<b>0.56</b>
Australia	0.40	0.40	0.40	0.40	0.60	0.60	0.40	0.40	1.00	1.00	1.50	1.50
North Africa	0.70	0.70	0.20	0.20	1.40	1.40	0.40	0.40	1.00	1.00	0.50	0.50
Sub-Saharan Africa	3.40	3.40	0.40	0.40	4.70	4.70	0.60	0.60	2.70	2.70	0.70	0.70
Middle East	0.50	<b>0.38</b>	0.10	0.10	1.40	1.31	0.30	0.30	1.70	<b>3.18</b>	0.60	0.60
Central America	1.40	1.40	0.60	0.60	1.20	1.20	0.80	0.80	1.40	1.40	1.40	1.40
South America	3.80	3.80	0.30	0.30	3.40	3.40	0.30	0.30	2.40	2.40	0.60	0.60
RBU	1.80	<b>1.18</b>	0.30	<b>0.08</b>	2.40	<b>1.36</b>	0.50	0.47	3.60	<b>5.10</b>	0.90	<b>1.17</b>
Central Asia	0.50	<b>0.32</b>	0.00	0.00	0.60	0.55	0.00	0.00	1.20	<b>1.88</b>	0.10	0.10
Antarctica	0.10	0.10	0.00	0.00	0.10	0.10	0.00	0.00	1.40	1.40	0.00	0.00
Continental	37.00	35.33	7.10	7.69	36.70	33.64	9.70	10.55	41.00	44.63	15.60	<b>17.10</b>
Open Oceans	9.90	11.86			12.90	15.43			26.90	27.18		
Global	46.90	47.19	7.10	7.69	49.60	49.07	9.70	10.55	67.90	71.81	15.60	<b>17.10</b>

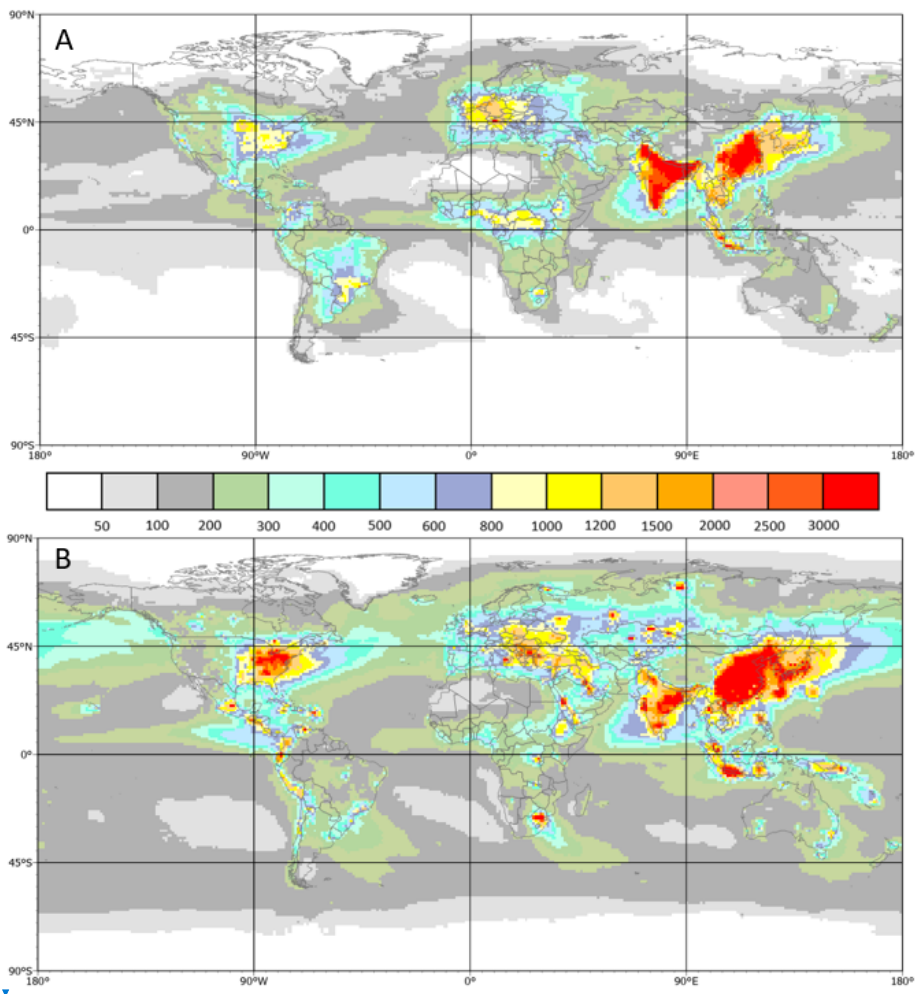
- Deleted: is
- Deleted: 70.65
- Deleted: 88
- Deleted: 59.4
- Deleted: 2
- Deleted: 130
- Deleted: 0
- Deleted: Most of this increase comes from a model in East Asia (Figure 2A).
- Deleted: 80
- Deleted:

Formatted: Font: 10 pt

Deleted: ¶

Region	Non-Coastal		Coastal		Non
	MMM	MMF	MMM	MMF	MMM
	<b>Total NH<sub>x</sub></b>				
North America	3.40	3.66	0.40	0.31	4.40
Europe	2.50	2.68	0.80	1.14	2.60
South Asia	8.60	8.60	1.00	1.00	3.60
East Asia	6.70	6.49	1.00	1.04	8.30
Southeast Asia	3.20	2.22	1.60	2.12	1.90
Australia	0.40	0.40	0.40	0.40	0.60
North Africa	0.70	0.70	0.20	0.20	1.40
Sub-Saharan Africa	3.40	3.40	0.40	0.40	4.70
Middle East	0.50	0.38	0.10	0.10	1.40
Central America	1.40	1.40	0.60	0.60	1.20
South America	3.80	3.80	0.30	0.30	3.40
RBU	1.80	1.18	0.30	0.08	2.40
Central Asia	0.50	0.32	0.00	0.00	0.60
Antarctica	0.10	0.10	0.00	0.00	0.10
Continental	37.00	35.33	7.10	7.69	36.70
Open Oceans	9.90	11.86			12.90
Global	46.90	47.19	7.10	7.69	49.60



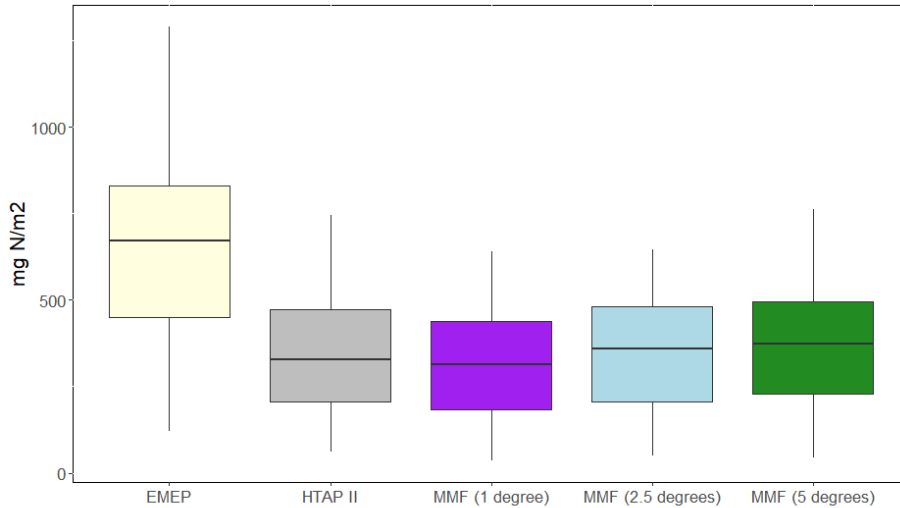


285  
 286 **Figure 2: Total N and S deposition in 2010 using the MMF approach. A)** Total annual N deposition (mg N/m<sup>2</sup>),  
 287 the sum of wet and dry NO<sub>3</sub><sup>-</sup> and NH<sub>4</sub><sup>+</sup> after applying the MMF approach, as well as HTAP II gridded surfaces of  
 288 dry deposition of NH<sub>3</sub>, HNO<sub>3</sub>, and NO<sub>2</sub> with no MMF adjustment due to the lack of measurements. **B)** Total S  
 289 deposition (mg S /m<sup>2</sup>), the sum of wet and dry MMF SO<sub>4</sub><sup>2-</sup> and wet and dry HTAP II SO<sub>2</sub>.

Deleted:

Deleted: wet and

Deleted: approach

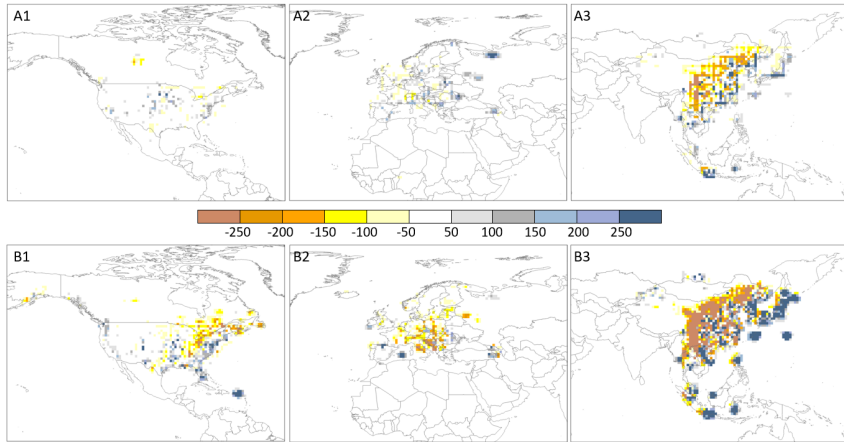


293  
 294 **Figure 3: A comparison between HTAP II, MMF, and EMEP wet deposition fluxes in Europe results at**  
 295 **EMEP observation sites.** A boxplot shows the distribution of EMEP, HTAP II, and MMF modeled wet reactive  
 296 nitrogen deposition (NH<sub>x</sub> and NO<sub>x</sub>) results at each EMEP observation location. Three different interpolation  
 297 distances are compared using MMF, 1 degree, 2.5 degrees, and 5 degrees.

298 Tan et al. (2018) report that their MMM underestimates the high observations of total N  
 299 deposition at some EMEP stations in Europe. We find that our 2.5° interpolation value for  
 300 European wet N deposition (8.0 Tg) is increased by 12.5% relative to the MMM surface (7.1  
 301 Tg), although the distance to the observations remains high (Figure 3). Figures 4, S4 and S5  
 302 show the difference between HTAP-II MMM and MMF nitrogen and sulfur deposition in North  
 303 America, Europe, and Asia in mg/m<sup>2</sup> with different interpolation distances. As the interpolation  
 304 distance increases, locations with a single measurement that is very different from the model will  
 305 influence the surrounding grid cells to be higher than the model. This effect is in particular  
 306 pronounced for sulfur deposition in Southeast Asia (Figure 4 B3) where the MMF procedure  
 307 increases deposition by up to 250 mg/m<sup>2</sup> relative to the MMM values.

308

- ~~Deleted:~~ is underestimating
- ~~Formatted:~~ Left
- ~~Deleted:~~ 7.9908
- ~~Deleted:~~ very
- ~~Deleted:~~ similar
- ~~Deleted:~~
- ~~Deleted:~~ 0
- ~~Deleted:~~ higher
- ~~Deleted:~~ are better reproduced with
- ~~Deleted:~~ M
- ~~Deleted:~~ MF
- ~~Deleted:~~ ¶
- ~~Deleted:~~ (e.g. sulfur observations in Southeast Asia, Figure 4-B3)
- ~~Deleted:~~ influence
- ~~Deleted:~~
- ~~Deleted:~~ ¶
- ~~Formatted:~~ Superscript



325

326 **Figure 4. The difference between MMF and MMM deposition with a 2.5-degree interpolation distance. A)**  
 327 **MMF minus MMM reactive nitrogen deposition in North America (A1) Europe (A2) and East Asia (A3) in mg/m<sup>2</sup>.**  
 328 **B) MMF minus MMM sulfate deposition in North America (B1) Europe (B2) and East Asia (B3) in mg/m<sup>2</sup>.** [Results](#)  
 329 [for other interpolation distances are shown in Figures S4 and S5, respectively.](#)

330

331 The spatial distribution is slightly different, with more deposition in coastal areas in the MMF  
 332 estimate (Table 2). Tan et al. (2018) report that the HTAP II MMM overestimates NO<sub>3</sub><sup>-</sup> wet  
 333 deposition in North America, but underestimates NH<sub>4</sub><sup>+</sup> deposition. We find that the MMF  
 334 interpolated deposition slightly improves these estimates, although the spatial distribution is very  
 335 similar [with the MMM](#) (Figures 2, 5). The largest change for S deposition (comparing MMM  
 336 and MMF) is in grid cells classified as ocean because of an increase in East and Southeast Asia  
 337 deposition which mostly occurs in areas classified as ocean due to the small island size [relative](#)  
 338 [to the coarse](#) spatial resolution [of the models](#). We note that, [ocean](#) cells were classified as such if  
 339 they were located further than 1<sup>o</sup> from the mainland; therefore, any islands smaller than 1<sup>o</sup> were  
 340 counted as [the](#) ocean.

341

342

Deleted: O

Deleted: Tan et al.,

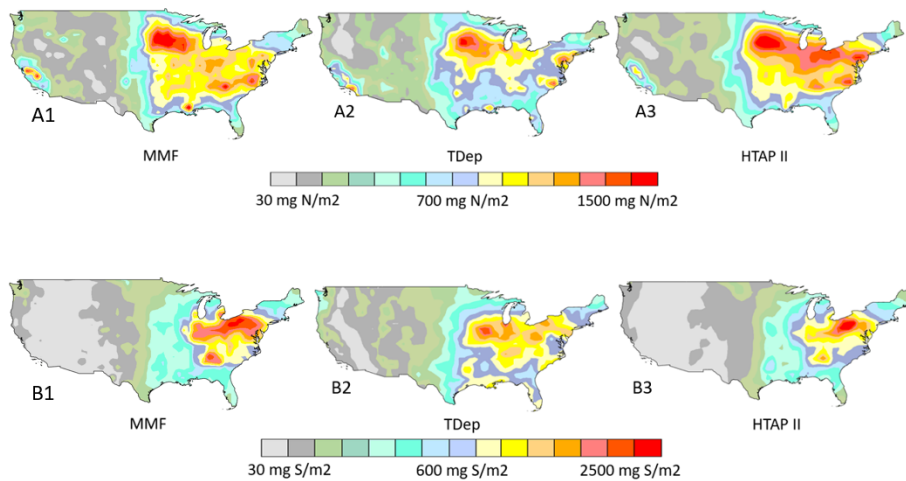
Deleted: and low

Deleted: O

Deleted: degree

Deleted: degree

Deleted: The largest change for S deposition is in continental grid cells due to an increase in East Asia.



351

352 **Figure 5: 2010 Total N deposition in the continental USA. A)** Total N is modeled with 1) MMF (this work), 2)  
 353 TDep annual map available from the NADP and 3) Tan et al.'s 2018 MMM. **B)** 2010 SO<sub>x</sub> wet deposition in the US  
 354 as modeled with 1) MMF (this work), 2) TDep annual map available from the NADP, and 3) Tan et al.'s 2018  
 355 multi-model mean HTAP II output.

356

357 There are spatial differences between an aggregated 1° x 1° [version of](#) the original TDep map of  
 358 nitrogen deposition for the United States as available from the NADP (Figure 5A2), the HTAP II  
 359 [deposition](#) produced by Tan et al. (2018) corresponding to the same area, and the  
 360 deposition map produced in this work (Figure 5A1). A similar pattern is seen in the map of SO<sub>4</sub><sup>2-</sup>  
 361 [deposition](#) (Figure 5B1; 5B3; 5B3). [While the TDep maps have been aggregated to the 1x1](#)  
 362 [degree resolution of the HTAP fields, there is still different regional variation in the deposition](#)  
 363 [patterns in the TDep maps than the HTAP II maps. In particular, TDep is capturing higher west](#)  
 364 [coast values that HTAP II does not while showing lower values in the Midwest/New](#)  
 365 [York/Pennsylvania region.](#)

366 The R<sup>2</sup> value for the linear regression between MMF wet SO<sub>4</sub><sup>2-</sup> and observed wet SO<sub>4</sub><sup>2-</sup> in the US  
 367 is [0.64](#) (Figure 6). The R<sup>2</sup> value for the linear regression between the HTAP II wet SO<sub>4</sub><sup>2-</sup> and  
 368 observed SO<sub>4</sub><sup>2-</sup> is [0.060](#), and [0.89](#) for the linear regression between the TDep wet SO<sub>4</sub><sup>2-</sup> and  
 369 observed SO<sub>4</sub><sup>2-</sup> (Figure 6). This means that TDep is better reproducing the NADP/NTN

Formatted: Font: Bold

Deleted: surface

Deleted: Tan et al.,

Deleted: NH<sub>4</sub>

Deleted: NH

Deleted: 0.76

Deleted: NH

Deleted: NH

Deleted: 66

Deleted: 92

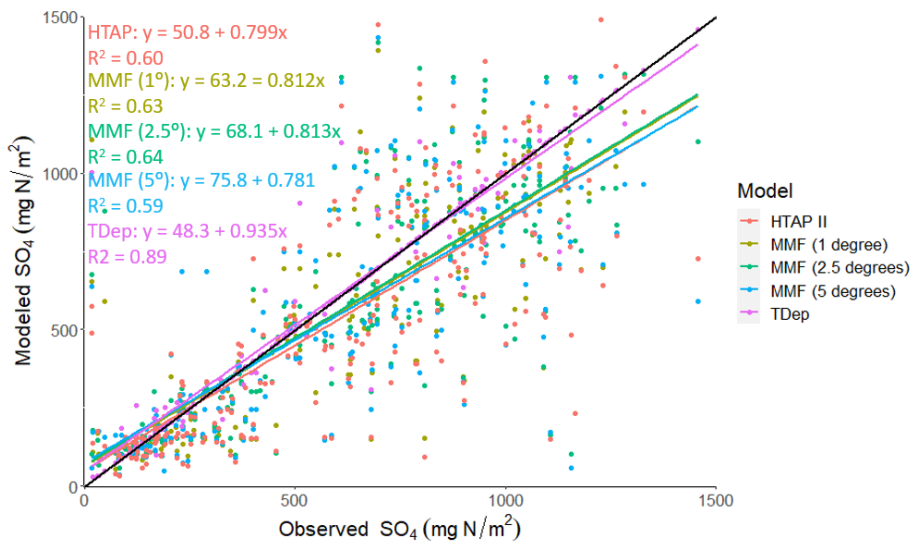
Deleted: NH

Deleted: NH

381 measurements and their spatial differences, whereas the MMF fields remain more similar to the  
 382 HTAP II ensemble model output. The higher TDep R<sup>2</sup> value likely occurs because of the finer  
 383 mesh (12 km) used in the TDep product, the closer proximity to individual stations as compared  
 384 to HTAP II used in the MMF approach, and the ability of the regional model to capture  
 385 gradients. In principle, emissions should be the same but in global models they are averaged over  
 386 larger areas. All three datasets produce similar values to the measured wet SO<sub>x</sub> deposition at the  
 387 NADP/NTN sites (Figure 6). The NH<sub>4</sub> and NO<sub>3</sub> wet deposition values are shown in  
 388 supplemental figures S2 and S3, and have much lower correlations (for all three interpolation  
 389 distances), with an R<sup>2</sup> of 0.1 for NO<sub>3</sub> and 0.53 for NH<sub>4</sub> at a 2.5° weighted distance.

Deleted: methodology  
 Deleted: is  
 Deleted: and  
 Deleted: and showing  
 Deleted: r2 xx  
 Deleted: y  
 Deleted: , yy  
 Deleted: 4, and zz for N,  
 Deleted: degree  
 Deleted: .

390



391

392 **Figure 6: Observed and modeled wet SO<sub>4</sub><sup>2-</sup> deposition in the US in 2010.** Each NADP/NTN wet deposition  
 393 measurement and the associated HTAP II, TDep, or MMF NH<sub>x</sub> wet deposition modeled value, with all values  
 394 shown together in A. The black line is the 1:1 line. Similar plots are shown in Figures S2 and S3 for wet NO<sub>3</sub> and  
 395 wet NH<sub>4</sub>.

Deleted: NH<sub>4</sub>  
 Formatted: Font: 10 pt, Bold  
 Deleted: .

396

## 397 5. Discussion

### 398 5.1 Consistency of MMF deposition with global emission estimates.

411 Geddes et al. (2017) used satellite observations to report global NO<sub>y</sub> emissions of 57.5 Tg-N/yr  
412 in 2010, similar to the 60.4 Tg-N emissions reported by HTAP II. This matches well with our  
413 total global MMF-derived NO<sub>y</sub> deposition (58.1 Tg-N). HTAP II ammonia emissions were 59.3  
414 Tg-N, slightly lower than the MMF NH<sub>3</sub> and NH<sub>4</sub><sup>+</sup> deposition of 62.3 Tg-N. The total MMM  
415 sulfur emissions for 2010 were 90.7 Tg S, very similar to the MMF sulfur deposition of 88.9 Tg-  
416 N.

### 417 5.2 Deposition over China.

418 A promising data set of wet deposition measurements (NO<sub>3</sub><sup>-</sup>, NH<sub>4</sub><sup>+</sup>, and SO<sub>4</sub><sup>2-</sup>) in China is  
419 available through the National Nitrogen Deposition Monitoring Network (NNDMN (Xu et al.,  
420 2019)). It is comparable to other regional measurements (Wen et al., 2020). However, these data  
421 only exist for a fraction of 2010 (from September onwards) for a few sites; rather than use partial  
422 data to represent an entire year, these sites were not included in our study. Research in China  
423 (Liu et al., 2020) analyzed the spatial pattern of N deposition by combining satellite observations  
424 with NNDMN deposition measurements (Xu et al., 2019); they found a 2012 average of 18.21 kg  
425 N ha<sup>-1</sup> for China. Additional work combining the GEOS-Chem  
426 (<http://acmg.seas.harvard.edu/geos/>) model with satellite observations and surface measurements  
427 reports the average annual deposition from 2008-2012 as 16.4 Tg-N with 10.2 Tg-N from NH<sub>x</sub>  
428 and 6.2 Tg-N from NO<sub>y</sub> (Zhao et al., 2017). The averages reported by these studies are consistent  
429 with ours (16.9 kg · ha<sup>-1</sup> · yr<sup>-1</sup>) despite the difference in year and spatial resolution. The spatial  
430 pattern of N deposition in 2010 (Figure 2A) also remains similar to that of previous decades (Jia  
431 et al., 2014), with high deposition in eastern China and low deposition over the Tibetan Plateau.  
432 This pattern is confirmed in 2006 and 2013 (Qu et al., 2017).

### 433 5.3 Limitations of interpolation.

434 As seen in Table 2, the largest difference between MMM and MMF is found in coastal regions  
435 and particularly the open ocean. While MMF does give improved deposition estimates by  
436 incorporating in-situ measurements, it is worth considering the scale of the model. Observations  
437 of deposition are probably not everywhere representative for a 1° or larger resolution and  
438 observations of precipitation may also not be homogenous in all directions at that scale,  
439 especially over heterogeneous terrain. So, for example, the coarse resolution of the model, even  
440 with added measurements is likely not accurately capturing gradients between coastal and inland

Deleted: Geddes and Martin,

Deleted: 59.4

Deleted: However, it suggests that either emissions for HTAP II models' simulations are too low, or deposition is too high since presumably the global deposition should be similar to the emissions.

Deleted: 51.93

Deleted: substantially

Deleted:

Deleted: 70.65

Deleted: 26

Deleted: strongly suggesting that emissions are too low, or deposition is too high.

Deleted: somewhat larger than the computed

Deleted: 80

Deleted: 1

Formatted: Abstract

Deleted: explored

Deleted: analysed

Deleted: observations

Deleted: .

Deleted: 88

Deleted: 17.24

Deleted: slight

Deleted: timeframe

Deleted: in our study.

Formatted: Font: Italic

Formatted: Font: Italic

Deleted: better

Deleted: varying

Deleted: the

469 deposition. While higher resolution precipitation values are available in some regions (e.g.,  
470 PRISM in the US), there is still a dearth of both wet and dry deposition measurements. Even on  
471 the North American continental scale, Schwede et al. (2011) showed that partially overlapping  
472 dry deposition estimates from CASTNET (USA) and CAPMoN (Canada) can be very different,  
473 despite using similar methodologies. This adds uncertainty to the dry deposition data (though  
474 there are very few dry deposition estimates included in this study) and emphasizes the  
475 importance of understanding deposition velocity model methodology.

Deleted: e.g.

476 The differences between the TDep, MMM, and MMF gridded deposition (Figure 5) are clearly  
477 visible in the center of the US. While the general patterns of deposition are similar for the three  
478 products, the magnitude of deposition in the aggregated TDep dataset (1° x 1°) is higher in the  
479 eastern US and lower in the western US than either of the other two deposition fields. This  
480 difference is likely due to the precipitation dataset used to calculate wet deposition. The MMF  
481 deposition is based on the MMM dataset; therefore, both utilize the same precipitation dataset,  
482 from a combination of 11 global models. However, TDep wet deposition is produced by  
483 multiplying PRISM precipitation data and an interpolated gridded surface dataset of wet NH<sub>4</sub><sup>+</sup>  
484 concentrations. PRISM is a reanalysis product designed to interpolate precipitation in  
485 particularly complex landscapes using weather radar and rainfall gauge observations, though it is  
486 not identical to observations because it used long-term averages as predictor grids (Zhang et al.,  
487 2018). It captures much more localized variation in precipitation due to geographical variations  
488 which are not captured in the lower resolution global precipitation models used in the HTAP II  
489 MMM (Tan et al., 2018a). To illustrate this, we compare PRISM to the available Community  
490 Atmosphere Model with Chemistry (<https://www2.acom.ucar.edu/gcm/cam-chem>, “CAM-  
491 Chem”), which was one of the models in the HTAP II ensemble. Subtracting the CAM-Chem  
492 precipitation output over the US from aggregated PRISM precipitation shows that CAM-Chem  
493 greatly underestimates precipitation volume in the US in 2010 (Figure S6). We note, however,  
494 that this comparison does not take differences in precipitation frequency between the model and  
495 observations into account. This matters because if the difference in precipitation volume comes  
496 from a few large magnitude storms, it will not influence the overall wet deposition values much.  
497 This is a good example of the differences that occur when comparing global and regional climate  
498 models and serves to emphasize the importance of resolving spatial and temporal scales. The

Deleted: in the US

Deleted: middle of the country

Deleted: 1

503 total deposition within the US borders is similar for the MMF, HTAP II, and aggregated TDep  
504 gridded surfaces; however, the spatial distribution is different.

505 MMF and MMM deposition distributions are similar because MMF is based on HTAP II.  
506 Likewise, the MMF results are similar to the TDep values at observation locations because,  
507 despite the difference in precipitation, both utilize the same NADP/NTN measurements to  
508 constrain the models. The key difference between MMF, when compared to MMM, is that  
509 measurement locations are not centered in each 1° x 1° grid cell; therefore, the center of each grid  
510 cell (the value compared to the observation, by interpolation to the station location) will not  
511 exactly equal the measured deposition but will instead be equal to the measurements weighted  
512 proportionally to distance from the centroid. This means that the graphical comparison of Figure  
513 6 is showing the actual measurement locations and 3 different model results with some  
514 meaningful influence from measurements that are nonetheless unique values, except in the very  
515 rare instance that the measurement corresponds exactly to the center of a grid cell. [Figure 6](#)  
516 [shows a stronger correlation for SO<sub>4</sub> than Figures S2 and S3 do for the nitrogen species. This](#)  
517 [could be related to the relatively shorter timescales of NO<sub>y</sub> and NH<sub>x</sub> in the atmosphere. The](#)  
518 [relatively coarse resolution of the global models cannot deal with these gradients, so the shorter](#)  
519 [timescales are reflected in the observations which are therefore less representative for the larger](#)  
520 [grid scales of the models.](#)

521 TDep maps of North American nitrogen deposition created with Schwede and Lear's  
522 methodology (2014), using IDW, are widely in use and freely available from the NADP. [The](#)  
523 [sensitivity analysis demonstrates that as the interpolation distance increases, the influence of the](#)  
524 [observations on the HTAP II grid increases, smoothing some of the artifacts that can occur using](#)  
525 [a small interpolation distance \(Figures 6, S2, S3\). In this respect it is worth mentioning that the](#)  
526 [original TDep dataset for North America used a maximum distance of 30 km plus half the cell](#)  
527 [size of PRISM \(2.07 km\). While it is not entirely clear how this distance was determined,](#)  
528 [operational factors such as the station density and the grid size of the regional model are likely](#)  
529 [important factors. In contrast, the maximum distances explored in this study are much larger \(1°,](#)  
530 [2.5°, 5°\) and are more adapted to the grid size of the current generation of global atmospheric](#)  
531 [chemistry transport models, and considerations of transport distances of atmospheric](#)  
532 [components. From our analysis there is no obvious better weighting distance that improves the](#)  
533 [comparison with observations. An adaptive distance weighting that considers the expected](#)

**Deleted:**  
**Formatted:** Subscript

**Deleted:** with

**Deleted:** to mention

**Deleted:** d

**Deleted:**

**Formatted:** Not Strikethrough

**Deleted:** d

**Deleted:** is

**Deleted:** 5x5; 2.5x2.5 and 1x1 degrees

**Deleted:** is



543 gradients between the observation point and the remote model grid could be explored as a way  
544 forward.

Deleted: ,

545 However, there are strong limitations associated with using IDW (Sahu et al., 2010), and other  
546 interpolation methods such as kriging or geographically weighted regression could provide  
547 smoother surfaces with fewer artifacts. IDW is a fast and flexible interpolation method, but it  
548 does not minimize error and can produce inaccurate results in regions with sparse measurements  
549 and large sub-grid variability. This problem is relevant to much of the world. The lack of  
550 measurement sites globally is a hindrance that can be alleviated by including information  
551 obtained from satellite remote sensing (Walker et al., 2019). Future work should also investigate  
552 methods such as machine learning techniques with spatial information to avoid these limitations.

Deleted: ly

Deleted: sensed

Deleted: observations

553 These results from measurement-model fusion are important because previous methods on a  
554 global scale have relied primarily on models (Vet et al., 2014; Tan et al., 2018a). They compare  
555 their results with measurements, of course, in order to demonstrate the model capabilities but  
556 they do not explicitly incorporate point measurements into the final product. Our results serve to  
557 emphasize that global models are adequately simulating deposition (in terms of total deposition  
558 budgets) but that the regional discrepancies between models and measurements can still be quite  
559 large; and measurement-model fusion helps to ameliorate this without changing the fundamental  
560 model parameters and processes that actually capture the overall deposition reasonably well.

Deleted: the

## 561 6. Conclusions

562 Sulfur and nitrogen deposition remain a serious concern for human and ecosystem health. We  
563 update the 2010 deposition budgets using measurement-model fusion to combine the broad  
564 spatial coverage of a model with accurate in-situ measurements. The total nitrogen deposition  
565 budget is recalculated to 114.50 Tg-N and the sulfur budget is recalculated to 88.91 Tg-N,  
566 representing about a 1% and 6.5% increase, respectively, from the modelled values. This work  
567 emphasizes the necessity of combining models with observations wherever possible, to better  
568 capture regional patterns and to inform policy and decision-making. Future work to improve  
569 measurement-model fusion should investigate more advanced MMF methods to avoid the  
570 limitations associated with IDW such as surface artifacts and high error in regions with sparse  
571 measurements. It could also incorporate satellite remote sensing derived concentrations to

Deleted: s

Deleted: 130

Deleted: 80

Deleted: 9

Deleted: other

Deleted: methods of interpolation

Deleted: should

Deleted: imagery

585 improve model estimates where in-situ measurements are not available, but a careful error  
586 analysis is needed to avoid spurious results.

Deleted: .  
Deleted:

589 **Author Contribution**

590 HR carried out the methods and analyzed the results. JSF and FD designed the project. HR  
591 prepared the manuscript with contributions from JSF and FD. RL, KH, and HF provided data.

592 **Competing Interests**

593 The authors declare no competing interests.

594 **Code Availability**

595 Data analysis was done using ArcMap Desktop 10.8.1, ArcGIS Pro, and R (R Core Team, 2022).

596

597 **References**

- 598 Adon, M., Galy-Lacaux, C., Yoboué, V., Delon, C., Lacaux, J. P., Castera, P., Gardrat, E.,  
599 Pienaar, J., Al Ourabi, H., Laouali, D., Diop, B., Sigha-Nkamdjou, L., Akpo, A., Tathy, J. P.,  
600 Lavenu, F., and Mougin, E.: Long term measurements of sulfur dioxide, nitrogen dioxide,  
601 ammonia, nitric acid and ozone in Africa using passive samplers, *Atmos. Chem. Phys.*, 10,  
602 7467–7487, <https://doi.org/10.5194/acp-10-7467-2010>, 2010.
- 603 Anderson, D. M., Burkholder, J. M., Cochlan, W. P., Glibert, P. M., Gobler, C. J., Heil, C. A.,  
604 Kudela, R. M., Parsons, M. L., Rensel, J. E. J., Townsend, D. W., Trainer, V. L., and Vargo, G.  
605 A.: Harmful algal blooms and eutrophication: Examining linkages from selected coastal regions  
606 of the United States, *Harmful Algae*, 8, 39–53, <https://doi.org/10.1016/j.hal.2008.08.017>, 2008.
- 607 Acid Deposition Monitoring Network in East Asia (EANET): <https://www.eanet.asia/>, last  
608 access: 18 November 2021.
- 609 Bobbink, R., Hicks, K., Galloway, J., Spranger, T., Alkemade, R., Ashmore, M., Bustamante,  
610 M., Cinderby, S., Davidson, E., Dentener, F., Emmett, B., Erismann, J.-W., Fenn, M., Gilliam, F.,  
611 Nordin, A., Pardo, L., and Vries, W. D.: Global assessment of nitrogen deposition effects on  
612 terrestrial plant diversity: a synthesis, *Ecological Applications*, 20, 30–59,  
613 <https://doi.org/10.1890/08-1140.1>, 2010.
- 614 Bowman, W. D., Cleveland, C. C., Halada, L., Hreško, J., and Baron, J. S.: Negative impact of  
615 nitrogen deposition on soil buffering capacity, *Nature Geoscience*, 1, 767–770,  
616 <https://doi.org/10.1038/ngeo339>, 2008.
- 617 Clark, C. M., Bai, Y., Bowman, W. D., Cowles, J. M., Fenn, M. E., Gilliam, F. S., Phoenix, G.  
618 K., Siddique, I., Stevens, C. J., Sverdrup, H. U., and Throop, H. L.: Nitrogen Deposition and  
619 Terrestrial Biodiversity, in: *Encyclopedia of Biodiversity*, Elsevier, 519–536,  
620 <https://doi.org/10.1016/B978-0-12-384719-5.00366-X>, 2013.
- 621 Dentener, F., Drevet, J., Lamarque, J. F., Bey, I., Eickhout, B., Fiore, A. M., Hauglustaine, D.,  
622 Horowitz, L. W., Krol, M., Kulshrestha, U. C., Lawrence, M., Galy-Lacaux, C., Rast, S.,  
623 Shindell, D., Stevenson, D., Noije, T. V., Atherton, C., Bell, N., Bergman, D., Butler, T., Cofala,  
624 J., Collins, B., Doherty, R., Ellingsen, K., Galloway, J., Gauss, M., Montanaro, V., Müller, J. F.,  
625 Pitari, G., Rodriguez, J., Sanderson, M., Solmon, F., Strahan, S., Schultz, M., Sudo, K., Szopa,  
626 S., and Wild, O.: Nitrogen and sulfur deposition on regional and global scales: A multimodel  
627 evaluation, *Global Biogeochemical Cycles*, 20, <https://doi.org/10.1029/2005GB002672>, 2006.
- 628 Dise, N. B. and Stevens, J.: Nitrogen deposition and reduction of terrestrial biodiversity:  
629 Evidence from temperate grasslands, *Sci. China Ser. C.-Life Sci.*, 48, 720–728,  
630 <https://doi.org/10.1007/BF03187112>, 2005.
- 631 Doney, S. C., Mahowald, N., Lima, I., Feely, R. A., Mackenzie, F. T., Lamarque, J.-F., and  
632 Rasch, P. J.: Impact of anthropogenic atmospheric nitrogen and sulfur deposition on ocean  
633 acidification and the inorganic carbon system, *PNAS*, 104, 14580–14585,  
634 <https://doi.org/10.1073/pnas.0702218104>, 2007.

635 European Monitoring and Evaluation Programme (EMEP): <https://www.emep.int/>, last access: 18  
636 November 2021.

637 Canadian Air and Precipitation Monitoring Network: [https://www.canada.ca/en/environment-](https://www.canada.ca/en/environment-climate-change/services/air-pollution/monitoring-networks-data/canadian-air-precipitation.html)  
638 [climate-change/services/air-pollution/monitoring-networks-data/canadian-air-precipitation.html](https://www.canada.ca/en/environment-climate-change/services/air-pollution/monitoring-networks-data/canadian-air-precipitation.html),  
639 last access: 18 November 2021.

640 Fu, J. S., Carmichael, G. R., Dentener, F., Aas, W., Andersson, C., Barrie, L. A., Cole, A., Galy-  
641 Lacaux, C., Geddes, J., Itahashi, S., Kanakidou, M., Labrador, L., Paulot, F., Schwede, D., Tan,  
642 J., and Vet, R.: Improving Estimates of Sulfur, Nitrogen, and Ozone Total Deposition through  
643 Multi-Model and Measurement-Model Fusion Approaches, *Environ. Sci. Technol.*, 56, 2134–  
644 2142, <https://doi.org/10.1021/acs.est.1c05929>, 2022.

645 Galy-Lacaux, C., Delon, C., Solmon, F., Adon, M., Yoboué, V., Mphepya, J., Pienaar, J. J.,  
646 Diop, B., Sigha, L., Dungall, L., Akpo, A., Mougin, E., Gardrat, E., and Castera, P.: Dry and Wet  
647 Atmospheric Nitrogen Deposition in West Central Africa, in: Nitrogen Deposition, Critical  
648 Loads and Biodiversity, edited by: Sutton, M. A., Mason, K. E., Sheppard, L. J., Sverdrup, H.,  
649 Haeuber, R., and Hicks, W. K., Springer Netherlands, Dordrecht, 83–91,  
650 [https://doi.org/10.1007/978-94-007-7939-6\\_10](https://doi.org/10.1007/978-94-007-7939-6_10), 2014.

651 Geddes, J. A. and Martin, R. V.: Global deposition of total reactive nitrogen oxides from 1996 to  
652 2014 constrained with satellite observations of NO<sub>2</sub> columns, *Atmospheric Chemistry and*  
653 *Physics*, 17, 10071–10091, <https://doi.org/10.5194/acp-17-10071-2017>, 2017.

654 Heisler, J., Glibert, P. M., Burkholder, J. M., Anderson, D. M., Cochlan, W., Dennison, W. C.,  
655 Dortch, Q., Gobler, C. J., Heil, C. A., Humphries, E., Lewitus, A., Magnien, R., Marshall, H. G.,  
656 Sellner, K., Stockwell, D. A., Stoecker, D. K., and Suddleson, M.: Eutrophication and harmful  
657 algal blooms: A scientific consensus, *Harmful Algae*, 8, 3–13,  
658 <https://doi.org/10.1016/j.hal.2008.08.006>, 2008.

659 INDAAF – International Network to study Deposition and Atmospheric chemistry in Africa:  
660 <https://indaaf.obs-mip.fr/>, last access: 18 November 2021.

661 Jia, Y., Yu, G., He, N., Zhan, X., Fang, H., Sheng, W., Zuo, Y., Zhang, D., and Wang, Q.:  
662 Spatial and decadal variations in inorganic nitrogen wet deposition in China induced by human  
663 activity, *Sci Rep*, 4, 3763, <https://doi.org/10.1038/srep03763>, 2014.

664 Kicklighter, D. W., Melillo, J. M., Monier, E., Sokolov, A. P., and Zhuang, Q.: Future nitrogen  
665 availability and its effect on carbon sequestration in Northern Eurasia, *Nat Commun*, 10, 3024,  
666 <https://doi.org/10.1038/s41467-019-10944-0>, 2019.

667 Labrador, L., Volosciuk, C., and Cole, A.: Measurement-Model Fusion for Global Total  
668 Atmospheric Deposition, a WMO initiative, World Meteorological Organization, 2020.

669 Lamarque, J.-F., Dentener, F., McConnell, J., Ro, C.-U., Shaw, M., Vet, R., Bergmann, D.,  
670 Cameron-Smith, P., Dalsoren, S., Doherty, R., Faluvegi, G., Ghan, S. J., Josse, B., Lee, Y. H.,  
671 MacKenzie, I. A., Plummer, D., Shindell, D. T., Skeie, R. B., Stevenson, D. S., Strode, S., Zeng,  
672 G., Curran, M., Dahl-Jensen, D., Das, S., Fritzsche, D., and Nolan, M.: Multi-model mean

673 nitrogen and sulfur deposition from the Atmospheric Chemistry and Climate Model  
674 Intercomparison Project (ACCMIP): evaluation of historical and projected future changes,  
675 *Atmos. Chem. Phys.*, 13, 7997–8018, <https://doi.org/10.5194/acp-13-7997-2013>, 2013.

676 Li, R., Cui, L., Zhao, Y., Zhang, Z., Sun, T., Li, J., Zhou, W., Meng, Y., Huang, K., and Fu, H.:  
677 Wet deposition of inorganic ions in 320 cities across China: spatio-temporal variation, source  
678 apportionment, and dominant factors, *Atmospheric Chemistry and Physics*, 19, 11043–11070,  
679 <https://doi.org/10.5194/acp-19-11043-2019>, 2019.

680 Liu, L., Zhang, X., Xu, W., Liu, X., Zhang, Y., Li, Y., Wei, J., Lu, X., Wang, S., Zhang, W.,  
681 Zhao, L., Wang, Z., and Wu, X.: Fall of oxidized while rise of reduced reactive nitrogen  
682 deposition in China, *Journal of Cleaner Production*, 272, 122875,  
683 <https://doi.org/10.1016/j.jclepro.2020.122875>, 2020.

684 Lu, Z., Streets, D. G., Zhang, Q., Wang, S., Carmichael, G. R., Cheng, Y. F., Wei, C., Chin, M.,  
685 Diehl, T., and Tan, Q.: Sulfur dioxide emissions in China and sulfur trends in East Asia since  
686 2000, *Atmos. Chem. Phys.*, 10, 6311–6331, <https://doi.org/10.5194/acp-10-6311-2010>, 2010.

687 Luo, X. S., Tang, A. H., Shi, K., Wu, L. H., Li, W. Q., Shi, W. Q., Shi, X. K., Erisman, J. W.,  
688 Zhang, F. S., and Liu, X. J.: Chinese coastal seas are facing heavy atmospheric nitrogen  
689 deposition, *Environ. Res. Lett.*, 9, 095007, <https://doi.org/10.1088/1748-9326/9/9/095007>, 2014.

690 National Atmospheric Deposition Program: <https://nadp.slh.wisc.edu/>, last access: 18 November  
691 2021.

692 Qu, L., Xiao, H., Zheng, N., Zhang, Z., and Xu, Y.: Comparison of four methods for spatial  
693 interpolation of estimated atmospheric nitrogen deposition in South China, *Environ Sci Pollut*  
694 *Res*, 24, 2578–2588, <https://doi.org/10.1007/s11356-016-7995-0>, 2017.

695 R Core Team: R: A Language and Environment for Statistical Computing, 2022.

696 Sahu, S. K., Gelfand, A. E., and Holland, D. M.: Fusing point and areal level space–time data  
697 with application to wet deposition, *Journal of the Royal Statistical Society: Series C (Applied*  
698 *Statistics)*, 59, 77–103, <https://doi.org/10.1111/j.1467-9876.2009.00685.x>, 2010.

699 Schwede, D., Zhang, L., Vet, R., and Lear, G.: An intercomparison of the deposition models  
700 used in the CASTNET and CAPMoN networks, *Atmospheric Environment*, 45, 1337–1346,  
701 <https://doi.org/10.1016/j.atmosenv.2010.11.050>, 2011.

702 Schwede, D., Cole, A., Vet, R., and Lear, G.: Ongoing U.S. - Canada Collaboration on Nitrogen  
703 and Sulfur Deposition, 5, 2019.

704 Schwede, D. B. and Lear, G. G.: A novel hybrid approach for estimating total deposition in the  
705 United States, *Atmospheric Environment*, 92, 207–220,  
706 <https://doi.org/10.1016/j.atmosenv.2014.04.008>, 2014.

707 Sirois, A.: The effects of missing data on the calculation of precipitation-weighted-mean  
708 concentrations in wet deposition, *Atmospheric Environment. Part A. General Topics*, 24, 2277–  
709 2288, [https://doi.org/10.1016/0960-1686\(90\)90321-D](https://doi.org/10.1016/0960-1686(90)90321-D), 1990.

710 Tan, J., Fu, J. S., Dentener, F., Sun, J., Emmons, L., Tilmes, S., Sudo, K., Flemming, J., Jonson,  
711 J. E., Gravel, S., Bian, H., Davila, Y., Henze, D. K., Lund, M. T., Kucsera, T., Takemura, T., and  
712 Keating, T.: Multi-model study of HTAP II on sulfur and nitrogen deposition, *Atmospheric  
713 Chemistry and Physics*, 18, 6847–6866, <https://doi.org/10.5194/acp-18-6847-2018>, 2018a.

714 Tan, J., Fu, J. S., Dentener, F., Sun, J., Emmons, L., Tilmes, S., Flemming, J., Takemura, T.,  
715 Bian, H., Zhu, Q., Yang, C.-E., and Keating, T.: Source contributions to sulfur and nitrogen  
716 deposition – an HTAP II multi-model study on hemispheric transport, *Atmospheric Chemistry  
717 and Physics*, 18, 12223–12240, <https://doi.org/10.5194/acp-18-12223-2018>, 2018b.

718 Tørseth, K., Aas, W., Breivik, K., Fjæraa, A. M., Fiebig, M., Hjellbrekke, A. G., Lund Myhre,  
719 C., Solberg, S., and Yttri, K. E.: Introduction to the European Monitoring and Evaluation  
720 Programme (EMEP) and observed atmospheric composition change during 1972 - 2009,  
721 *Atmospheric Chemistry and Physics*, 12, 5447–5481, <https://doi.org/10.5194/acp-12-5447-2012>,  
722 2012.

723 Clean Air Status and Trends Network (CASTNET): <https://www.epa.gov/castnet>, last access: 18  
724 November 2021.

725 Vet, R., Artz, R. S., Carou, S., Shaw, M., Ro, C.-U., Aas, W., Baker, A., Bowersox, V. C.,  
726 Dentener, F., Galy-Lacaux, C., Hou, A., Pienaar, J. J., Gillett, R., Forti, M. C., Gromov, S., Hara,  
727 H., Khodzher, T., Mahowald, N. M., Nickovic, S., Rao, P. S. P., and Reid, N. W.: A global  
728 assessment of precipitation chemistry and deposition of sulfur, nitrogen, sea salt, base cations,  
729 organic acids, acidity and pH, and phosphorus, *Atmospheric Environment*, 93, 3–100,  
730 <https://doi.org/10.1016/j.atmosenv.2013.10.060>, 2014.

731 de Vries, W., Solberg, S., Dobbertin, M., Sterba, H., Laubhann, D., van Oijen, M., Evans, C.,  
732 Gundersen, P., Kros, J., Wamelink, G. W. W., Reinds, G. J., and Sutton, M. A.: The impact of  
733 nitrogen deposition on carbon sequestration by European forests and heathlands, *Forest Ecology  
734 and Management*, 258, 1814–1823, <https://doi.org/10.1016/j.foreco.2009.02.034>, 2009.

735 Walker, J. T., Beachley, G., Amos, H. M., Baron, J. S., Bash, J., Baumgardner, R., Bell, M. D.,  
736 Benedict, K. B., Chen, X., Clow, D. W., Cole, A., Coughlin, J. G., Cruz, K., Daly, R. W.,  
737 Decina, S. M., Elliott, E. M., Fenn, M. E., Ganzeveld, L., Gebhart, K., Isil, S. S., Kerschner, B.  
738 M., Larson, R. S., Lavery, T., Lear, G. G., Macy, T., Mast, M. A., Mishoe, K., Morris, K. H.,  
739 Padgett, P. E., Pouyat, R. V., Puchalski, M., Pye, H. O. T., Rea, A. W., Rhodes, M. F., Rogers,  
740 C. M., Saylor, R., Scheffe, R., Schichtel, B. A., Schwede, D. B., Sexstone, G. A., Sive, B. C.,  
741 Sosa Echeverría, R., Templer, P. H., Thompson, T., Tong, D., Wetherbee, G. A., Whitlow, T. H.,  
742 Wu, Z., Yu, Z., and Zhang, L.: Toward the improvement of total nitrogen deposition budgets in  
743 the United States, *Science of The Total Environment*, 691, 1328–1352,  
744 <https://doi.org/10.1016/j.scitotenv.2019.07.058>, 2019.

745 Wen, Z., Xu, W., Li, Q., Han, M., Tang, A., Zhang, Y., Luo, X., Shen, J., Wang, W., Li, K., Pan,  
746 Y., Zhang, L., Li, W., Collett, J. L., Zhong, B., Wang, X., Goulding, K., Zhang, F., and Liu, X.:

747 Changes of nitrogen deposition in China from 1980 to 2018, *Environment International*, 144,  
748 106022, <https://doi.org/10.1016/j.envint.2020.106022>, 2020.

749 Xu, W., Luo, X. S., Pan, Y. P., Zhang, L., Tang, A. H., Shen, J. L., Zhang, Y., Li, K. H., Wu, Q.  
750 H., Yang, D. W., Zhang, Y. Y., Xue, J., Li, W. Q., Li, Q. Q., Tang, L., Lu, S. H., Liang, T.,  
751 Tong, Y. A., Liu, P., Zhang, Q., Xiong, Z. Q., Shi, X. J., Wu, L. H., Shi, W. Q., Tian, K., Zhong,  
752 X. H., Shi, K., Tang, Q. Y., Zhang, L. J., Huang, J. L., He, C. E., Kuang, F. H., Zhu, B., Liu, H.,  
753 Jin, X., Xin, Y. J., Shi, X. K., Du, E. Z., Dore, A. J., Tang, S., Collett, J. L., Goulding, K., Sun,  
754 Y. X., Ren, J., Zhang, F. S., and Liu, X. J.: Quantifying atmospheric nitrogen deposition through  
755 a nationwide monitoring network across China, *Atmos. Chem. Phys.*, 15, 12345–12360,  
756 <https://doi.org/10.5194/acp-15-12345-2015>, 2015.

757 Xu, W., Zhang, L., and Liu, X.: A database of atmospheric nitrogen concentration and deposition  
758 from the nationwide monitoring network in China, *Sci Data*, 6, 51,  
759 <https://doi.org/10.1038/s41597-019-0061-2>, 2019.

760 Zhang, M., Leon, C. de, and Migliaccio, K.: Evaluation and comparison of interpolated gauge  
761 rainfall data and gridded rainfall data in Florida, USA, *Hydrological Sciences Journal*, 63, 561–  
762 582, <https://doi.org/10.1080/02626667.2018.1444767>, 2018.

763 Zhang, Y., Foley, K. M., Schwede, D. B., Bash, J. O., Pinto, J. P., and Dennis, R. L.: A  
764 Measurement-Model Fusion Approach for Improved Wet Deposition Maps and Trends, *Journal*  
765 *of Geophysical Research: Atmospheres*, 124, 4237–4251,  
766 <https://doi.org/10.1029/2018JD029051>, 2019.

767 Zhao, Y., Zhang, L., Chen, Y., Liu, X., Xu, W., Pan, Y., and Duan, L.: Atmospheric nitrogen  
768 deposition to China: A model analysis on nitrogen budget and critical load exceedance,  
769 *Atmospheric Environment*, 153, 32–40, <https://doi.org/10.1016/j.atmosenv.2017.01.018>, 2017.

770 Zhu, J., Chen, Z., Wang, Q., Xu, L., He, N., Jia, Y., Zhang, Q., and Yu, G.: Potential transition in  
771 the effects of atmospheric nitrogen deposition in China, *Environmental Pollution*, 258, 113739,  
772 <https://doi.org/10.1016/j.envpol.2019.113739>, 2020.

773